Fetal MRI at Higher Field Strength

Andreas Stadlbauer and Daniela Prayer

Contents

Abstract

› While fetal MRI has become a routine method at field strengths up to 1.5 T, the use of higher field strength is at an early stage. A higher signal-to-noise ratio is accompanied by a higher energy deposition. In addition, parameters of sequences have to be adjusted to achieve useful contrasts. Susceptibility effects and certain artifacts that increase with higher field strength have to be considered. The same is true for certain artifacts that maybe negligible at lower field strength. Special measures have to be taken to grant maternal and fetal safety. Due to the high resolution, MR imaging at 3 T is currently the method of choice in postmortem fetal imaging.

1 Introduction

At the introduction of magnetic resonance imaging (MRI) into clinical practice in the late1970s, the most MR systems on the market operated at a magnetic field strength of ≤0.6 T. In these early days of MRI, a necessity for the development of more powerful magnets for imaging of parts of the body beyond the brain was commonly not seen. The first 1.5 T MR systems were introduced in 1982 and became the predominant magnetic field strength used for clinical high-quality MR imaging in the late 1980. At that time, MR scanners operating at 1.5 T were named "high-field systems." The first 3.0 T whole-body MR systems were developed in the early 1990s. Due to practical reasons, e.g.,

A. Stadlbauer (✉)
MR Physics Group, Department of Radiology,
Landesklinikum St. Poelten, Propst Fuehrer Strasse 4,
3100 St. Poelten, Austria and
Department of Neurosurgery, University of Erlangen-Nürnberg,
Schwabachanlage 6, 91054 Erlangen, Germany
e-mail: andi@nmr.at

D. Prayer
Department of Radiology, Medical University of Vienna,
Waehringer Gürtel 18–20, 1090 Vienna, Austria
e-mail: daniela.prayer@meduniwien.ac.at

D. Prayer (ed.) *Fetal MRI*, Medical Radiology,
DOI: 10.1007/174_2010_27, © Springer-Verlag Berlin Heidelberg 2011

inadequacies in radiofrequency (RF) coil design and protocols, installations of these systems remained limited to academic institutions for research till the beginning of the new century. However, a multiplicity of publications demonstrated improvements at 3.0 T in anatomical imaging (Duewell et al. 1996; Fujii et al. 1998; Ugurbil et al. 1993; Vinitski and Griffey 1991), MR spectroscopy (MRS) (Barfuss et al. 1990; Hetherington et al. 1995), and functional MRI (fMRI) (Jesmanowicz et al. 1998; Kruger et al. 2001; Menon et al. 1995; Thulborn 1999) – only a small sample of papers are presented here – compared with 1.5 T.

Safety guidelines of the Food and Drug Administration (FDA) which limited the magnetic field strength that may be used for diagnostic purposes were expanded from 2.0 to 4.0 T in 2002. The FDA limit for magnetic field for MR imaging applications in human subjects is currently at 8.0 T. Since that time and due to technological advances occurred meanwhile, 3.0 T whole-body MR systems have been introduced into clinical practice in increasing numbers and are the "high-field systems" of today, while MR systems operating at field strengths of below 1.5 T have generally lost popularity and are limited now to open designs.

The main argument for purchasing a 3.0 T MR system, besides commercial considerations (i.e., strategic marketing and to stay competitive), is the expected improvement in image quality due to increased signal-to-noise ratio (SNR) of up to twofold (Edelstein et al. 1986) compared to 1.5 T. This gain in SNR can be used directly to improve the image quality or traded for improved temporal or spatial resolution, or both. However, the transition to higher field strength was accompanied with new challenges, such as increases in RF power deposition (i.e., specific absorption rate, SAR), T1 relaxation times, RF effects, susceptibility effects, and chemical shift effects.

As mentioned above, important technological developments occurred besides the shift to the use of higher field main magnetic field strengths. These advances in MR technology include the development of phased array surface coils consisting of 4–16 or more coil elements, increased number and bandwidth of receiver channels, improvements in gradient performance, and innovative and accelerated acquisition techniques (Hussain et al. 2005).

The purpose of the first part of this chapter is to review and discuss the opportunities and challenges of MR imaging in the abdomen at high magnetic field strength, i.e., 3.0 T in context of this chapter. The second part addresses the potential and limitations of 3.0 T MRI for the use in fetal diagnostics.

2 Opportunities and Challenges of Abdominal MR Imaging at Higher Field Strength

The increase of strength of the main magnetic field (B_0), e.g., from 1.5 to 3.0 T, influences several physical parameters which are essential for the quality of the MR images. Most of the physical effects of the higher magnetic field strength are not solely beneficial or disadvantageous, but represent rather two sides of the same coin. It is important to see these changes of the physical parameters in connection with the type of MR application. Therefore, a discussion about opportunities and challenges rather than advantages and disadvantages of MR imaging at higher field strength is preferable. This section describes the changes of the most important physical parameters and their effects on MR imaging at higher field strength.

2.1 Signal-to-Noise Ratio

The SNR describes the signal strength of a tissue or a part of the body on the MR image relative to the background noise, which is defined as the mean standard deviation of the signal strength in the background of the image. The SNR is proportional to the net spin vector, also named as net magnetization. This net magnetization is defined as the difference between the number of spins aligned parallel and antiparallel to the main magnetic field, respectively, and increases almost linearly with increasing main magnetic field strength (Hoult and Phil 2000; Wen et al. 1997). At 1.5 T and under in vivo conditions (i.e., body temperature), five out of one million spins are additionally aligned along the magnetic field. This number, and hence the net magnetization, is double at 3.0 T, which creates the potential for a doubling of the derived signal. Since noise is independent of field strength and based on the arguments mentioned above, the SNR at 3.0 T should be double that at 1.5 T.

However, the SNR of an MR image depends not only on the field strength alone, but also on several of other parameters, e.g., the number of hydrogen spins per voxel volume (i.e., spatial resolution), acquisition time, receiver bandwidth, and the environment of the spins (i.e., relaxation effects). Equation (1) represents a simplified correlation between the SNR in spin-echo (SE) sequences and these parameters (Edelstein et al. 1986):

$$\mathrm{SNR}_{\mathrm{SE}} \propto B_0 \cdot V \cdot \sqrt{\frac{N_{\mathrm{ex}} \cdot N_{\mathrm{ph}}}{\mathrm{BW}}} \cdot (1 - e^{-\mathrm{TR}/T1}) \cdot e^{-\mathrm{TE}/T2}. \quad (1)$$

B_0 is the strength of the static magnetic field, V is the volume of a voxel, N_{ex} is the number of excitations, N_{ph} is the number of phase-encoding lines in k-space, and BW is the receiver bandwidth. The product of N_{ex} and N_{ph} is a measure of the image acquisition time. The two factors including exponential functions consider the effects of relaxation: TR and TE are the repetition and the echo time, T1 and T2 are the relaxation times, respectively. The equation for gradient-echo sequences is very similar, but showed two additional factors to account for flip angels <90° used for excitation and those <180° used for refocusing (Edelstein et al. 1986). Based on this formula, SNR is proportional to the main magnetic field strength, the voxel volume, the square root of the data acquisition time divided by the receiver bandwidth, and some tissue- (T1 and T2 relaxation time) and sequence-specific (TR and TE) terms. Provided that the other parameters in Eq (1) remain constant, the SNR at 3.0 T is really double that at 1.5 T. However, in real life these factors are usually affected by the field strength and tend unfortunately to counteract the benefit in SNR. At higher field strengths, the two most important effects, which lead to a limitation of the SNR advantage, are the increases in tissue T1 relaxation time values and the increased deposition of RF energy (i.e., SAR). The corrections to overcome these and other obstacles, which will be described in more detail in the following sections of this chapter, are mostly associated with a loss in SNR. The realized gain in SNR for abdominal MRI at 3.0 T over that at 1.5 T was reported to be between 0.8 and 5.6-fold (Merkle and Dale 2006; Merkle et al. 2006). Within a particular examination, the higher SNR afforded by higher field strength can be exploited in several different ways: to reduce acquisition time at a given spatial resolution or vice versa and variable combinations of the two.

A second aspect of SNR at higher field strength has to be discussed in this context. The beneficial increase in SNR at 3.0 T is associated with an increased noticeability of artifacts. Bernstein et al. (2006) called this phenomenon an increased artifact-to-noise ratio (ANR) due to the increased SNR. Some artifacts are masked by the noise on the image at 1.5 T. They are either not conspicuous or at least not troublesome because their intensity level is comparatively low. The increased ANR at higher field strength is associated with an increased background contrast and hence an increased detectability of the artifact. A typical example is Gibbs ringing (or truncation artifact) which tends to be more prominent at 3.0 T (Amartur and Haacke 1991; Dietrich et al. 2008). Gibbs ringing arises when the acquired raw data are clipped at the edges of k-space. In this case the signal intensities are significant over the level of noise at the border of k-space due to the increased SNR at higher field strength. Strategies to reduce or overcome the artifact are either to increase the spatial resolution, which is associated with an increase in measurement time and a decrease in SNR (see eq. 1), or the application of an apodization filter (e.g., Hanning filter).

2.2 B_0 Homogeneity and Susceptibility Effects

The homogeneity of the main (static) magnetic field (B_0) is a fundamental concern during the design and implementation of many magnetic resonance experiments, especially for echo planar imaging (EPI), steady-state free precession (SSFP), and localized MRS. The B_0 homogeneity has influence on the distribution of the resonance frequency of the protons and the linearity of the magnetic field gradients required for spatial encoding. The homogeneity depends on the passive and active shimming (a procedure to improve homogeneity) of the magnet, the composition and geometry of the object or subject under investigation, and any foreign (metal) objects in the subject or the scanner. At 3.0 T, it is more challenging to obtain a sufficient homogeneity of the main magnetic field. This kind of magnets requires more and high-order shimming.

A heterogeneous magnetic field, also known as "poor shimming of the magnet," leads to different effects: (a) the dispersion of the resonance frequency

of the spins within a single voxel leads to an increased dephasing of the magnetization and a decrease in T2* relaxation time, which is also a measure for signal loss due to B_0 inhomogeneity (Haacke et al. 1989; Yablonskiy and Haacke 1994). In MRS experiments the line width of the peaks, i.e., the width of the metabolic signal in the MR spectrum, is increased and may cause a worse spectral resolution due to overlapping peaks. Further, water and lipid suppression may be ineffective and resulted in poor quality of the spectrum; (b) Stronger variations of the resonance frequency cause, on the one hand, intravoxel dephasing, which is associated with signal attenuation and geometric distortions, especially at EPI sequences (Merboldt et al. 2000; Ojemann et al. 1997). SSFP sequences are also very sensitive to off-resonance effects which can cause banding artifacts (Wieben et al. 2008). Figure 1 shows examples for massive banding artifacts in SSFP sequences measured at a woman with a triplet pregnancy. On the other hand, these frequency variations result in mismatch of the excitation frequency of chemically selective radiofrequency (RF) pulses. This leads to an incomplete fat saturation for the application of frequency-selective (spectral) fat suppression.

An interesting point is the fact that the B_0 homogeneity of the empty magnet is very high, but substantially reduced by positioning of the patient inside the magnet because of the patient's susceptibility. Magnetic susceptibility is the extent to which a material becomes magnetized when exposed to a magnetic field. The susceptibility varies substantially for different materials. A distinction is drawn between diamagnetic materials like water and biological tissue, which weaken the external magnetic field and have negative susceptibility; paramagnetic substances like gadolinium and titanium with positive susceptibility, which show an enhancement of field strength inside the material; and ferromagnetic materials (e.g., iron) with a strong positive susceptibility. The susceptibility of air is approximately zero. As a consequence of the differences in magnetic properties of the materials, additional magnetic fields of different strength are superposed to the originally very homogenous main magnetic field and lead to partly drastic decrease in field homogeneity. Microscopic magnetic field gradients and variations occur around the interface of regions with different susceptibility (i.e., bone – soft tissue; or air – soft tissue) and lead to the so-called susceptibility artifacts. As susceptibility of a material is proportional to field strength, the worsening effect on the field homogeneity as well as the microscopic field variations at 3.0 T is double that at 1.5 T. On the other hand, this effect is exploited at 3.0 T in improving the sensitivity of MR imaging sequences to the presence of hemorrhage and mineralization (Frayne et al. 2003).

A variety of protocol manipulations are available to minimize the influence of susceptibility artifacts:

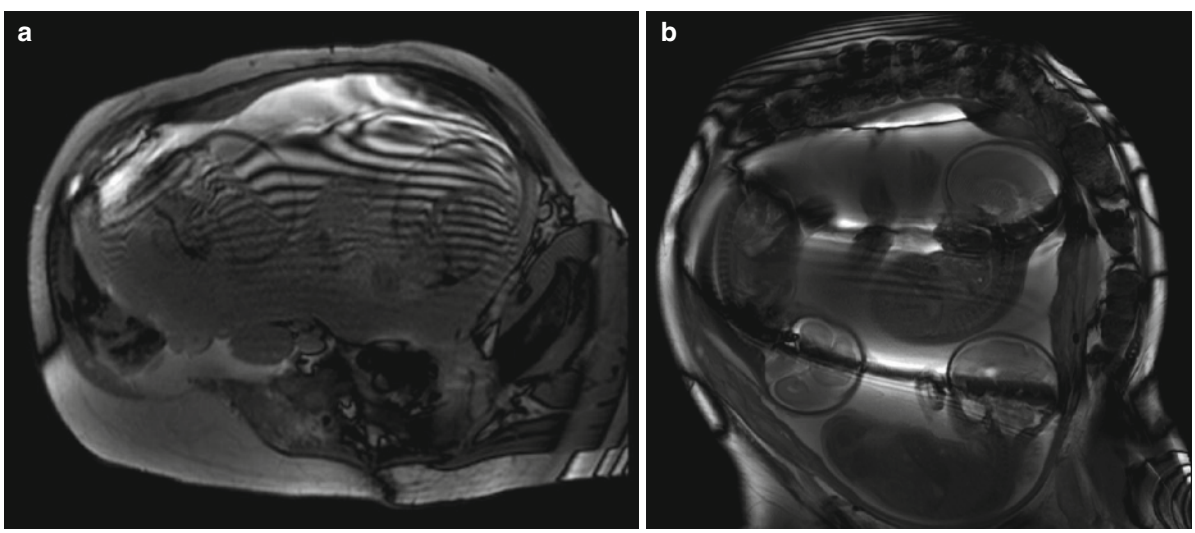

Fig. 1 Bending artifact in fetal MRI at higher field strength. Axial (**a**) and coronal (**b**) image of band-shaped signal losses (banding artifact) in steady-state free precession (SSFP) sequences due to B_0 inhomogeneities in a woman with a triplet pregnancy at 22 weeks of gestation measured at 3.0 T

shorter TE and/or increased receiver bandwidth, reductions in voxel size, or better shimming of the main magnetic field. The higher SNR that is afforded by 3.0 T also allows for the implementation of parallel imaging techniques within echo planar imaging, which shortens echo trains and helps to reduce these artifacts. An alternative method is the view-angle tilting method which is not widely used at the moment at 3.0 T, but has the drawback of increased image blurring (Butts et al. 2005; Cho et al. 1988).

2.3 Larmor Frequency and Chemical Shift

Larmor frequency (resonance frequency) linearly increases with magnetic field strength. At 1.5 T, the Larmor frequency of protons is 63.9 MHz and doubles to 127.8 MHz at 3.0 T. The higher resonance frequency is associated with both advantages (e.g., higher spectral resolution in MRS applications) and difficulties (e.g., increased chemical shift artifacts). Furthermore, the RF coils have to be tuned to the Larmor frequency of the MR system; hence, RF coils of a 1.5 T system cannot be used at 3.0 T.

Chemical shift artifacts are due to the difference in resonance frequency between water and fat. This difference is proportional to field strength, i.e., it is about 225 MHz at 1.5 T and 450 MHz at 3.0 T. A distinction is drawn between the chemical shift artifact of the first and the second kind. The chemical shift artifact of the first kind is a misregistration artifact and occurs only in frequency encoding and slice selection direction due to the slight difference between the precessional frequency of protons in water and fat, respectively. In other words, the proton spins of water at one location precess at the same frequency as the proton spins of fat at another location. Consequently, the images arise from the water and the fat signals are superposed and shifted in frequency direction which leads to a hyperintense line at one side and a hypointense line on the opposite side of the organ. The width of the lines increases with field strength. The artifact can be reduced by increasing the receiver bandwidth (Hussain et al. 2005); however, this strategy is related with a reduction of the SNR. Alternatively, the view-angle tilting mentioned above or a fat-suppression technique can be helpful, which in turn leads to an increase of acquisition time and/or an increase in RF deposition (SAR). The increased chemical shift between water and fat, however, has the advantage of more effective spectral fat suppression.

The difference in Larmor frequency between water and fat is associated with a reduction of the time period until proton spins of water and fat precess in phase, i.e., it is reduced from 4.6 ms at 1.5 T to 2.3 ms at 3.0 T. This effect of higher field strength is known as the chemical shift artifact of the second kind. It is advantageous for MR imaging in the abdomen of opposed-phase echoes, which are used for fat suppression. The shortening of the in-phase period allows for a reduction of echo time and hence a reduction in acquisition time and artifacts. However, it might be a problem for pulse sequences that use in-phase echo times due to a more challenging timing of the RF pulses.

An important point regarding the RF pulses of imaging sequences at 3.0 T represents the fact that the RF pulses also have to match the higher resonance frequency. A higher frequency of the RF pulses is equivalent to a shorter wavelength of the RF pulses which is associated with today's most important challenges and technical difficulties related to abdominal MR imaging at higher field strength: increased inhomogeneities of the B_1 field, stronger heating of tissue due to increased RF deposition and SAR, and standing wave effects. These challenges and effects will be the topic of the following subsection.

2.4 B_1 Homogeneity, Standing Wave Effect, and RF Deposition

The RF field used in MR imaging is also referred to as B_1 field and its strength increases proportionally with main magnetic field strength. The purpose of the B_1 field is to excite the spins and create an MR signal that can be detected by a receiver coil. The wavelength of the RF field in air is approximately 468 cm at 1.5 T and 234 cm at 3.0 T. The dielectric constant (ε_r) is an important physical parameter in context of in vivo MR imaging. The higher the dielectric constant of a medium, the slower the speed of light through it and the shorter the wavelength becomes. The dielectric constant of air and water is about 1 and 80, respectively; that of human tissue can be assessed between 10 and 100 (Gabriel et al. 1996a, b, c). The wavelength in a medium is reduced by a factor calculated as the inverse of the square root of the dielectric constant,

i.e., $1/\sqrt{\varepsilon_r}$ (Tanenbaum 2006). This effect reduces the RF wavelength at 3.0 T from 234 cm in air to about 30 cm in water-containing tissue (Haacke et al. 1999). The wavelength of the RF field at 3.0 T is in the same scale as the size of the field-of-view (FOV) used in many abdominal MRI applications. As a result, regional brightening and signal loss due to constructive and destructive interference of the standing waves can be observed. These artifacts are called standing waves effects (formerly incorrectly called "dielectric resonance effect") (Collins et al. 2005) and tend to be more pronounced with increasing FOV as required in fetal MR imaging. A related artifact, which is known as conductivity artifact (Merkle et al. 2006), is caused by the interaction of the (rapidly changing) RF field and highly conductive tissue or liquids in the body. The RF field induces a circulating electric current, which on its part creates induced magnetic fields that oppose the change of the original magnetic field due to the Lenz's law. In other words, the induced circulating current acts like an electromagnet that attenuates the causing RF field. The more conductive the medium, the stronger is the opposing effect and the greater is the reduction of amplitude and dissipation of energy of the RF field. Therefore, large amounts of highly conductive amniotic or ascitic fluid can cause a substantial shielding effect and requires more RF power for compensation which in turn increases SAR.

These two effects, the standing wave artifact and the conductivity artifact, combine to cause particularly strong artifacts for abdominal MR imaging, especially in pregnant women at a late stage of gestation or women with a multiple pregnancy. Figure 2 shows an example for the combination of the standing wave and the conductivity artifact for a woman with a triplet pregnancy.

A simple method to reduce B_1 inhomogeneity and wave-related artifacts is to use multichannel phased array receive coils, which have a stronger B_1-sensitivity near the body surface and might partially counteract the standing wave and conductivity artifact. However, especially in abdominal MR imaging, the artifacts persist and image quality is not acceptable. Another possibility for correction, which is commercially available, is a B_1 receive-field correction that uses low-resolution maps from the body and surface coils can be applied (Narayana et al. 1988). These corrections go by various names, such as constant level appearance (CLEAR), phased array uniformity enhancement (PURE), and prescan normalization. However, these methods are postprocessing corrections and do not compensate for B_1 inhomogeneity. Improvement of RF penetration by positioning an additional "RF cushion" with high dielectric constant on the abdomen of the patient has been demonstrated (Franklin et al. 2008). However, this is not an acceptable and feasible solution, especially for pregnant women.

A promising and more advanced technique for compensation B_1 inhomogeneities uses multichannel transmission body coils (Vernickel et al. 2007), which allows for application of methods such as active shimming of the RF field (Ullmann et al. 2005) and local excitation in combination with parallel transmission methods (Zhu 2004), e.g., transmit sensitivity encoding (transmit SENSE) (Katscher et al. 2003). This technology was under intensive development during the last years and the first commercially available MR system was introduced recently (Achieva 3.0 T TX, Philips Medical Systems).

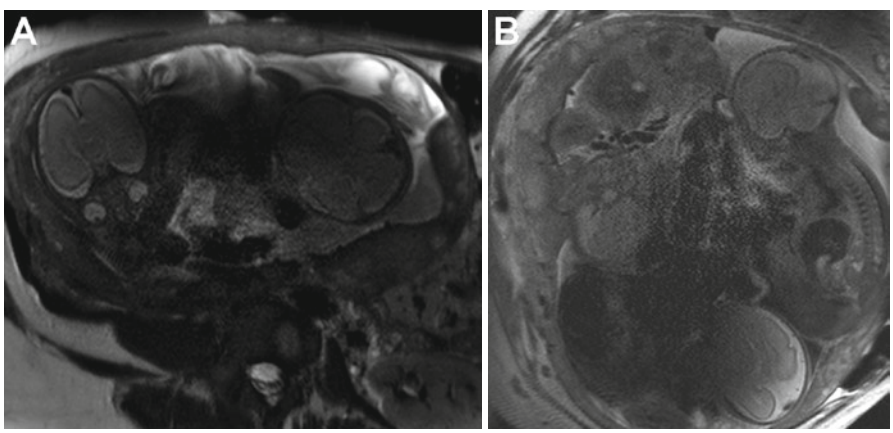

Fig. 2 Standing wave and conductivity artifact in fetal MRI at higher field strength. Axial (**a**) and coronal (**b**) image of a combined appearance of the standing wave and the conductivity artifact in T2-weighted turbo spin-echo (TSE) sequences in a woman with a triplet pregnancy at 22 weeks of gestation measured at 3.0 T

The SAR is a measure for the energy deposited in tissue by the RF pulses, or in other words, for the energy which is transferred via the RF flied into the patient's body where it generates heat. The SAR increases quadratically with the resonance frequency (i.e., the B_1 field strength) and the flip angle of the RF pulse. Among other factors, it additionally depends on the duty cycle of the RF pulses (i.e., the ratio between the RF pulse duration and the time period between two consecutive pulses), on the bandwidth of the RF pulses, and on the size and the position of the patient (Bernstein et al. 2006; Kuhl et al. 2008; Soher et al. 2007). The correlation between SAR and the bandwidth of the RF pulses is critical, because an increase of the bandwidth was recommended as favorable strategy to overcome susceptibility and chemical shift effects at the higher field strength. A doubling of the bandwidth of the RF pulses in combination with the inherent increase in SAR due to the higher B_1 field strength leads to a factor of eight for the net increase in SAR going from 1.5 to 3.0 T. In addition, the situation in pregnant women is twofold problematic. First, the standing wave artifact tends to be more pronounced and can result in inhomogeneous power deposition and formation of localized "hot spots" near or even in the fetus. Second, the huge amount of amniotic fluid leads to a greater RF field attenuation due to the conductivity artifact, and in turn, to an increased RF power for compensation in order to maintain signal intensity and image quality. However, an increase of the RF power is not possible when operating at the SAR limits. These effects and the relevance of the pregnancy-related SAR problems increase with increasing week of gestation. Therefore, intensified effort to cope with the increasing RF deposition, especially at late stage of gestation, is necessary. In an interesting study by Hand et al. (2006), the authors used an electromagnetic solver based on the time domain finite integration technique in combination with an anatomically realistic model of a pregnant woman at 28 weeks of gestation to predict SAR values in the mother and the fetus for 3.0 T MR systems. They found that the highest local SAR occurs in the mother. The maximum local SAR in the fetus was approximately 50–70% of that in the mother and occurred in a limb. This was due to the fact that relatively high SAR was exposed within the amniotic fluid and placenta close to the fetal limb. They concluded that their results suggest that control of the maternal maximum local SAR, rather than the whole-body averaged SAR, is required to comply with U.S. Food and Drug Administration (FDA) and International Commission on Non-Ionizing Radiation Protection (ICNIRP) guidelines.

The SAR as a limiting factor will be most relevant for RF-intensive MR protocols like turbo spin-echo (TSE), SSFP, or fat-saturated sequences. Conventional strategies to reduce increased RF deposition at 3.0 T compared to 1.5 T include protocol adjustment such as an increase of TR, decrease in the number of slices, decrease of the flip angle of the RF pulses, shorten the echo train length, and/or increase of inter echo spacing. However, all proposed solutions are associated with undesired penalties like increase in image acquisition time, reduction of anatomical coverage, changes in image contrast, and reduction of the gain in SNR at 3.0 T.

Parallel imaging (Griswold et al. 2002; Pruessmann et al. 1999) is a powerful method for reduction of SAR levels. These techniques allow for a reduction of the number of phase-encoding steps and shortening of image acquisition time, thereby leading to a reduction of RF energy absorbed and less tissue heating. A reduction factor (R) of two yields to a twofold reduction of RF deposition. However, an inherent drawback of all parallel imaging techniques is a decrease in SNR ($R=2$ reduces SNR by 40%), which is at least partly compensated by the higher signal at 3.0 T. Please refer to Chap. 2 for more details about the parallel imaging techniques.

More innovative modifications in pulse sequence design use different strategies for modulations of the flip angle of the refocusing pulses in TSE or gradient-echo sequences; these include flip angle sweep, hyperechoes, and transition between pseudo-steady states (TRAPS). Flip angle sweep (Morakkabati-Spitz et al. 2006) uses a successive reduction of the refocusing flip angle starting from the usual angle (e.g., 180°) to a much lower value (e.g., 130°) over the echo train. However, small refocusing angles give rise to the formation and interferences of the so-called stimulated echoes, and the prolongation of T1 relaxation times at 3.0 T (see next subsection for more detail) may lead to a mixed T1/T2 contrast, which has to be considered during interpretation of the images. A more advanced spin refocusing strategy uses varying flip angles and varying pulse phases which are symmetrically arranged around a central 180° pulse to completely refocus magnetization. This leads to the formation of echoes, thus hyperechoes (Hennig and Scheffler 2001; Weigel and Hennig 2006), and allows to preserve SNR as in conventional TSE sequences at simultaneous

reduction of SAR (up to 70–90%). Hyperechoes are complex signals consisting of several sources of magnetization, including transverse magnetization, longitudinal magnetization, and stimulated echo components of individual RF pulses; additionally, relaxation and diffusion effects have to be considered as well (Hussain et al. 2005). A drawback of hyperechoes is the fact that the echo time has to be increased to obtain T2 contrast which is similar to that provided by standard fast SE sequences. The TRAPS approach is based on the observation that once a static pseudo-steady state for a given refocusing flip angle is established, the maximum attainable signal is extremely robust against variations of the flip angles of the refocusing pulses. This technique allows for a significant reduction in RF power deposition for TSE sequences, by using higher flip angles only for the central part of k-space (Hennig et al. 2003).

2.5 Relaxation Time Effects

The longitudinal relaxation time T1 of many tissues increases with increasing strength main magnetic field but does not follow a simple mathematical correlation (Bottomley et al. 1984; de Bazelaire et al. 2004; Stanisz et al. 2005). T1 relaxation, which is also known as spin-lattice relaxation, describes the recovery process of the longitudinal magnetization by transfer of energy between the excited spins (protons in case of MR imaging) and the surrounding structure (also named as lattice, following the terminology of solid-state physics). The easier the energy transfer between the spins and the lattice occurs, the faster the longitudinal magnetization is recovered and the shorter is T1. As the strength of the main field B_0 increases, the resonance frequency of the spins as well as the energy which is required for a spin flip process (from parallel to antiparallel) also increases and, hence, the efficiency of the energy transfer decreases. This results in longer T1 relaxation times at 3.0 T. The reported results for the degree of T1 increase from 1.5 to 3.0 T demonstrates a wide range of measured changes, between up to 40% increase in skeletal muscle and up to 73% increase in kidney (Stanisz et al. 2005). The problems that are related to the increase in T1 relaxation times are a decrease in image SNR (please refer to the Sect. 2.1), a decrease in image contrast, and an increase in conspicuity of certain artifacts. Examples for a decreased image contrast at 3.0 T because of a different degree of T1 prolongation of two tissues are the gray matter-to-white matter contrast in MR imaging of the brain and the kidney-to-liver contrast in abdominal MR imaging. The increase in conspicuity of certain artifacts is related to the fact that the T1 relaxation time increases only by 10–20% [P4:3,43]. Therefore, the lipid signal remains stronger compared to the signal of other tissues at 3.0 T, leading to increased artifacts such as chemical shift artifacts or Gibbs ringing (Soher et al. 2007).

On the other hand, it was accepted that the transverse relaxation time T2 is mostly independent of the main magnetic field strength (Bernstein et al. 2006; Bottomley et al. 1984). T2 is the time constant for the decay of the transverse magnetization due to spin–spin interactions, hence also called spin–spin relaxation time. However, more recent studies (de Bazelaire et al. 2004; Gold et al. 2004; Stanisz et al. 2005) suggest a small but statistically insignificant decrease of T2 relaxation time in certain tissues by 10–15% as the field strength is increased from 1.5 to 3.0 T. Therefore and due to the afore-mentioned increased susceptibility effects at higher field strength, the apparent transverse relaxation time T2* decreases at 3.0 T. T2* is not a tissue-specific parameter like T1 or T2. Besides the T2 relaxation time, field inhomogeneities and susceptibility effects are included in T2*. To the best of our knowledge, changes in relaxation times for fetal MR imaging at 3.0 T are not published thus far, but are assumed to be comparable in scale with the described effects.

These changes in relaxation times lead to the fact that the contrast between various tissues on MR images measured at 3.0 T cannot be the same as known from standard 1.5 T MR images. Several changes of parameters (i.e., repetition time, receiver bandwidth, etc.) of the pulse sequences are available for compensation.

2.6 Safety Concerns and Acoustic Noise

Little specific data about safety issues in fetal MR imaging at higher field strength are available. In general, it is assumed that a higher magnetic field strength is related to an increased torque on ferromagnetic implants, increased risk of RF burns from RF coils or echocardiogram leads, and an increase in acoustic noise. The latter two are of special interest in fetal MR imaging. Careful handling of RF coils and other medical equipment (e.g., to avoid direct contact between the coil and patient's

skin) will be the best strategy to avoid RF burns. The noise level, on the other hand, increases with field strength and the higher performance of the gradient system used at higher field strengths (the noise occurs during the quick current alterations in the gradient coils) (Foster et al. 2000). Passive approaches, such as earplugs or headphones, are sufficient to protect the mother from the high acoustic noise levels. However, for protection of the fetus, a reduction in gradient performance and/or acoustically shielded vacuum-based bore liners are required (Tanenbaum 2006).

3 Fetal MR Imaging at Higher Field Strength

In consideration of the challenges that are connected with fetal MR imaging at higher magnetic field strengths and are described in the previous section, the question for reasonableness is legitimate. On the other hand, the chance to obtain increased SNR at higher field strength, which can be used for higher spatial resolution or faster imaging, is of course an issue of interest in fetal MR imaging. Therefore, research groups are busy with tuning of MR sequences as well as development of new MR hardware to take up the challenges. Initial experiences from a pilot study at the Department of Radiology of Medical University of Vienna demonstrated, however, that the way from 1.5 to 3.0 T in fetal MR imaging is challenging and not straight forward. Promising results from the first four patients are presented in the following two subsections of this chapter. All women had premature amniorrhexis which helps to reduce the intensity of the standing wave and the conductivity artifact. All measurements were performed on 3.0 T clinical whole-body MR scanners (Achieva, Philips Medical Systems, Best, The Netherlands or TRIO, Siemens Medical Solutions, Erlangen, Germany) using multichannel surface coils.

3.1 Fetal Diffusion-Weighted MR Imaging

Diffusion-weighted MR imaging (DWI) is a method for detection of the Brownian motion of water molecules and provides information about tissue structure and intra/extracellular space (Le Bihan et al. 2006). DWI sequences measure the signal attenuation which occurred due to diffusion of water molecules. The observed signal decay can be used to calculate the diffusion properties or the apparent diffusion coefficient (ADC).The essential parameters for the "diffusivity weighting" are the strength and timing of the diffusion gradients and can be expressed with the so-called "*b*-factor." One basic rule of DWI is: the higher the *b*-factor, the stronger the "diffusion-weighting" and the signal drop-off in areas with higher diffusion in the images, but the lower the SNR of the DWI data.

Except for the problems related to a low SNR, long acquisition time, vulnerability to motion of the fetus due to breathing of the mother as well as diffusion mimicking signal attenuations due to blood flow in the capillaries have to be resolved first before fetal DWI is feasible. The use of parallel imaging techniques in combination with an MR system working at 3.0 T and multichannels receiver may help overcome some of these difficulties. The higher SNR at 3.0 T allows for application of higher *b* values, which in turn are more sensitive to diffusion and less sensitive to transverse relaxation time (T2) and perfusion-related motion. In general, the quality of DWI images measured at 3.0 T is superior to that of diffusion-weighted (DW) images obtained at 1.5 T. However, the magnetic field inhomogeneities that degrade DW images are worse at 3.0 T. Figure 3 shows an example of a DWI examination of the brain of a fetus at 3.0 T.

The DWIBS approach (DWIBS stands for DW whole-body imaging with background body signal suppression) was developed by Takahara et al. (2004). DWIBS is a new technology of body DW MRI acquiring multiple, thin axial slices with a high number of signal averages during free breathing and STIR (short TI inversion recovery) fat suppression, which provides high-spatial-resolution images of various regions of the body and can be useful in detecting malignancies in the whole body. The usefulness of DWIBS for the detection of thoracic and abdominal lesions has been demonstrated in a few reports (Bohlscheid et al. 2008; Komori et al. 2007; Murtz et al. 2007; Stadlbauer et al. 2009). A study by Takahara et al. (2008) used DWIBS to introduce and assess DW MR neurography for imaging of the brachial plexus. Figure 4 shows an example of the application of the DWIBS technique for visualization of the spinal cord of a fetus.

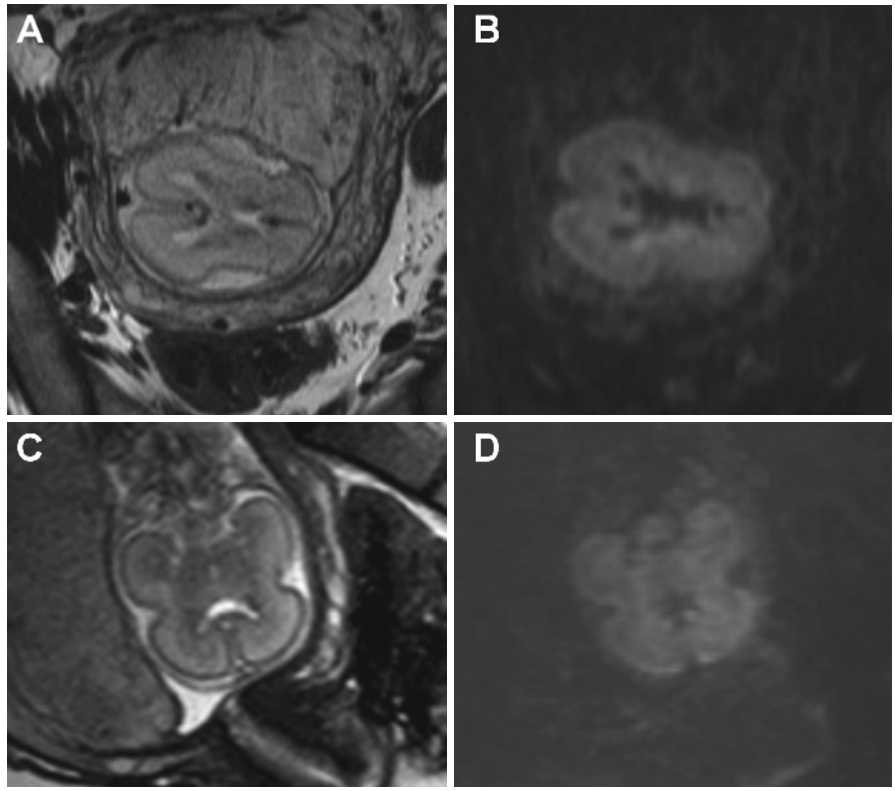

Fig. 3 Fetal diffusion-weighted MR imaging (DWI) at 3.0 T. Axial (**a**) and coronal (**c**) balanced steady-state free precession (balanced SSFP) images of a normally developed fetal brain (21 weeks of gestation). Corresponding axial (**b**) and coronal (**d**) DWI images measured with a *b*-value of 700 s/mm^2, an in-plane resolution of 1.3 × 1.3 mm^2, a slice thickness of 4 mm, and a TE/TR of 92/2,200 ms, respectively

Depending on the anatomical region, diffusion can occur unrestricted and equal in magnitude in all spatial directions, which is referred to as isotropic diffusion. However, mobility of water in biological tissue can show a preferred direction by structures, e.g., restriction of diffusion by myelinated sheets of nerve fibers, which is referred to as anisotropic diffusion. The conventional DWI method provides information about the magnitude of water diffusion but not about its direction.

Diffusion tensor MR imaging (DTI) allows for the measurement of anisotropic diffusion of water molecules in tissues such as white brain matter and provides insight into the microstructure of tissues (Le Bihan et al. 2001) with the use of diffusion gradients in at least six directions. DTI shows clinical application for preoperative planning of brain tumor surgery to differentiate peritumoral edema from tumor border, to assess tumor infiltration into white-matter tracts, and to visualize and localize the major white-matter tracts (Cruz and Sorensen 2006). This strategy can help to avoid injuries to normal and/or functionally important brain areas. Application of DWI and DTI is more problematic in regions outside of the brain, e.g., due to increased motion and susceptibility artifacts. However, these methods may provide helpful information regarding the development of the brain parenchyma and brain structures in a fetus as well as about the nature and extent of pathologies in several organs, which is currently a field of clinical investigations.

In general, DTI data are evaluated by calculating parametric maps of fractional anisotropy (FA) and mean diffusivity (MD) that describe the directionality and magnitude of water diffusion, respectively. Fiber tracking enables reconstruction of white matter pathways in three dimensions with the use of a mathematical algorithm for comparison of orientations of water diffusion anisotropy on a voxel-by-voxel basis. Reconstructed fiber bundles may be evaluated visually or with qualitative assessment. Figure 5 shows an example of a DTI examination and subsequent postprocessing using Fiber tracking of the DTI data of a fetus.

3.2 Fetal MR Venography

MR venography is a noninvasive imaging method for investigation of the vasculature of the human brain.

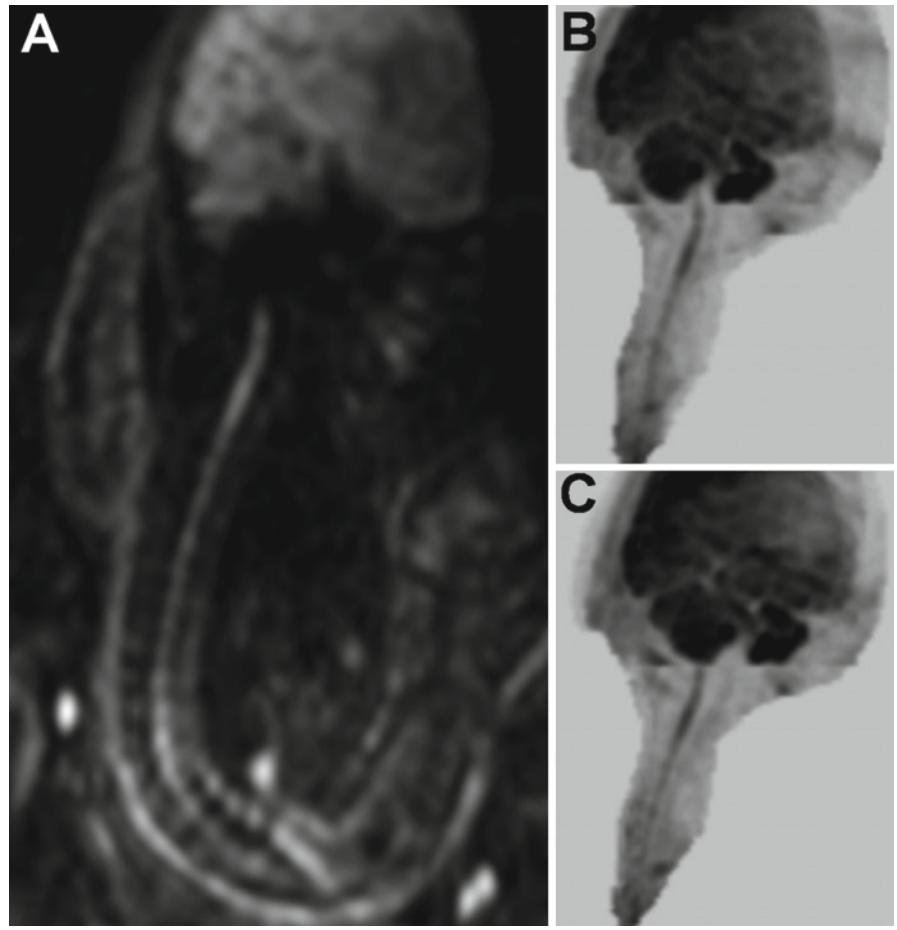

Fig. 4 Fetal diffusion-weighted whole-body imaging with background body signal suppression (DWIBS) at 3.0 T. Sagittal DWIBS image (**a**) of a fetus (30 weeks of gestation) measured with a *b*-value of 1,000 s/mm^2, an in-plane resolution of 1.5 × 1.5 mm^2, a slice thickness of 5 mm, and a TE/TR of 58/2,238 ms, respectively. Oblique sagittal maximum intensity projection (MIP) reconstructions and inversion of gray-scale for the DWIBS data (**b**) and (**c**)

A 3D gradient echo imaging technique to visualize venous structures has been introduced by Reichenbach et al. (1997, 1998). The underlying contrast mechanism of this method is based on the fact that the level of blood oxygenation of venous blood is smaller compared to arterial blood. The iron atom of deoxygenated hemoglobin contains four unpaired electrons and is paramagnetic for that reason. On the other hand, in oxygenated hemoglobin an oxygen molecule is attached to the iron atom, which leads to the fact that the electrons are not unpaired any longer, and consequently, the iron atom is diamagnetic. As described above, diamagnetic materials have negative susceptibility and weaken the external magnetic field, whereas paramagnetic substances have positive susceptibility. The paramagnetic nature of deoxygenated venous blood leads to magnetic field inhomogeneities and thus serves as a contrast media. These field inhomogeneities result in two effects: (a) a reduction of T2* (Li et al. 1998; Thulborn et al. 1982) and (b) a phase difference between the venous vessel and its surroundings (Gomori et al. 1987; Hoogenraad et al. 1998). In other words, the difference in oxygenation level between arterial and venous blood is associated with a difference in the bulk magnetic susceptibility of the blood in the vessel. Therefore, the intensity of this blood oxygenation level dependent (BOLD) susceptibility effect (or artifact) is higher at higher field strengths (Ogawa and Lee 1990; Turner et al. 1993) and MR venography benefits in general from higher field strengths. Figure 6 gives an example for an MR venography examination of a fetus and demonstrates the results of the subsequent postprocessing using minimum intensity projection of the MR venography data.

3.3 Postmortem Fetal MR Imaging

Solely MR studies at higher magnetic field strength (>1.5 T) on postmortem specimen of fetal brains were

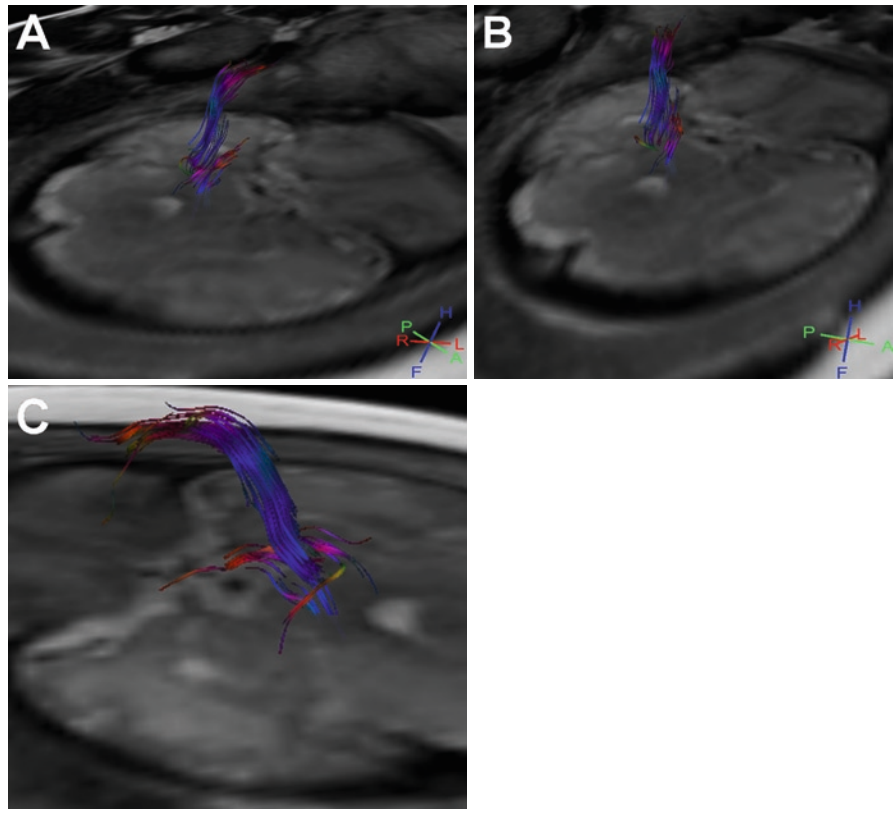

Fig. 5 Fetal diffusion tensor MR imaging (DTI) and fiber tracking at 3.0 T. Three-dimensional reconstruction of parts of the pyramidal tract as a result of a fiber tracking procedure of the DTI data using the FACT (fiber assignment by continuous tracking) algorithm. Reconstructed fiber tracts and DTI data were coregistered to transversal T2-weighted TSE images and depicted in (**a–c**) in three different projections. DTI data were measured on a normally developed fetal brain (30 weeks of gestation) using the following parameters: *b* values of 0 and 1,000 s/mm^2, diffusion gradients in 15 directions, in-plane resolution of 0.8×0.8 mm^2, slice thickness of 2.5 mm, and TE/TR of 55/4,100 ms

published in the literature so far. Sbarbati and coworkers (Sbarbati et al. 2004) investigated seven cadaveric human fetuses of gestational ages ranging from the 12th to the 16th week by acquiring 2D- and 3D T1- and T2-weighted MR images at a magnetic field strength of 4.7 T. The purpose of this study was to evaluate brain morphology in situ and to describe dynamics of brain development during an important period of fetal morphogenesis. MRI data were evaluated by 3D reconstruction and calculation of the thickness of the cortex in both hemispheres. The findings of the MR experiments were compared with histological sections obtained from ten paraffin-embedded brains from fetus of corresponding gestational age. The results of the 3D reconstruction of the MRI data demonstrated the increasing degree of maturation of the brains in terms of fronto-occipital distance, bitemporal distance, and occipital angle in all the fetuses and were quite similar to those provided by necropsy but with an absence of mechanical artifacts. A spatial in-plane resolution of 0.12×0.12 mm^2 voxel was sufficient for a detailed detection of five cortical layers and to visualize the subplate and marginal zones on T2-weighted MR images. The authors demonstrated with their paper the utility of MRI for studying brain development. They conclude that MR imaging with high spatial resolution at high field strength provides quantitative profiling of fetal brain, which allows for the calculation of important morphological parameters.

In a study by Huang et al. (2006) the authors acquired DTI data of postmortem fetal brain samples measured at 4.7 T. They evaluated the growth status of various white matter tracts on cross-sections at 19–20th gestational weeks and compared the findings with in vivo MR examinations of brains of 0-month-old neonates and 5- to 6-year-old children at 1.5 T. Limbic, commissural, association, and projection white matter tracts and gray matter structures were three-dimensionally reconstructed. They performed a quantitative characterization of these structures to assess their dynamic changes. Huang and coworkers found that the overall pattern of the time courses for the development of different white matter is that limbic fibers develop first and association fibers last and commissural and projection fibers are

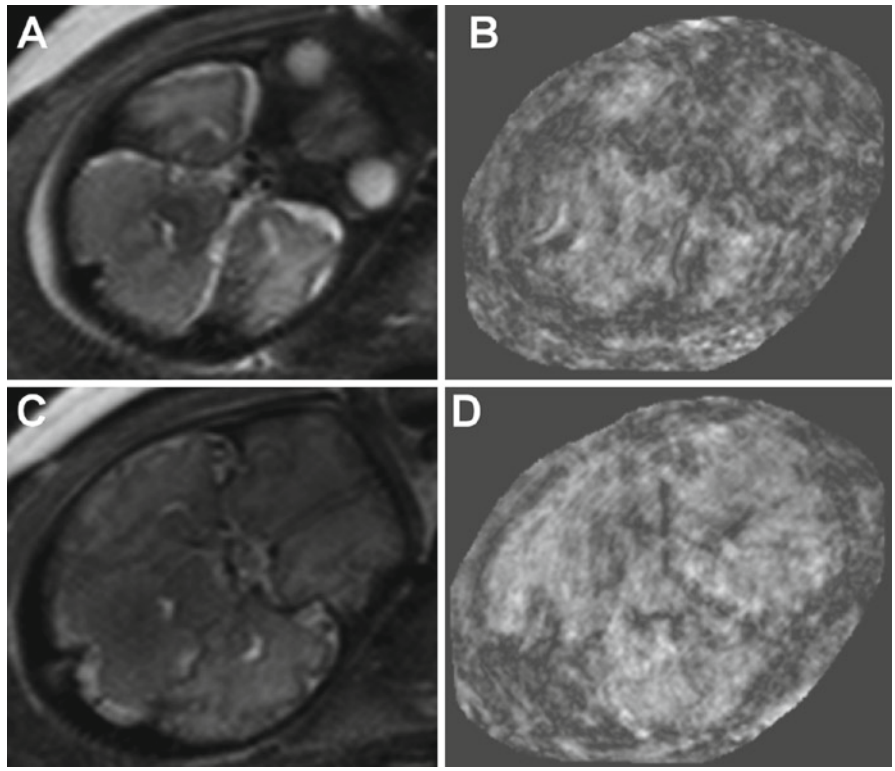

Fig. 6 Fetal MR venography at 3.0 T. Axial T2-weighted TSE images (**a**, **c**) of a normally developed fetal brain (30 weeks of gestation). Corresponding axial MR venography images after minimum intensity projection (mIP) reconstructions (**b**, **d**). MR venography data were measured using the following parameters: in-plane resolution of 0.45×0.45 mm^2, slice thickness of 2 mm, and TE/TR of 27/19 ms

forming from anterior to posterior part of the brain. Most white matter tracts have already formed at 0 month of age. They conclude that 3D DTI data of the human brain could be a valuable anatomical reference for diagnostic radiology of premature newborns as well as for basic human development studies.

Ren et al. (2006) analyzed midline glial and commissural development in postmortem human fetal brains ranging from 13 to 20 weeks of gestation using both DTI and immunohistochemistry. Fetal brains of between 14 and 16 weeks of gestation were scanned in a MR scanner working at field strength of 11.7 T. Brains of 17 weeks or older fetuses were scanned at 4.7 T. Their data show the morphological development of multiple forebrain commissures/decussations, including the corpus callosum, anterior commissure, hippocampal commissure, and the optic chiasm. Furthermore, they were able to demonstrate that mechanisms regulating callosal formation in the developing human brain are very similar to their findings of previous study about the developing mouse forebrain. Histological analyses performed in their studies showed that all the midline glial populations as well as structures analogous to the subcallosal sling and cingulate pioneering axons, which mediate callosal axon guidance in mouse, are also present during human brain development. They concluded from their data that similar mechanisms and molecules required for midline commissure formation operate during both mouse and human brain development. Therefore, the mouse is an excellent model system for studying normal and pathological commissural formation in human brain development.

References

Amartur S, Haacke EM (1991) Modified iterative model based on data extrapolation method to reduce Gibbs ringing. J Magn Reson Imaging 1:307–317

Barfuss H, Fischer H, Hentschel D, Ladebeck R, Oppelt A, Wittig R, Duerr W, Oppelt R (1990) In vivo magnetic resonance imaging and spectroscopy of humans with a 4 T whole-body magnet. NMR Biomed 3:31–45

Bernstein MA, Huston J III, Ward HA (2006) Imaging artifacts at 3.0T. J Magn Reson Imaging 24:735–746

Bohlscheid A, Nuss D, Lieser S, Busch HP (2008) Tumor search with diffusion-weighted imaging–first experience. Rofo 180:302–309

Bottomley PA, Foster TH, Argersinger RE, Pfeifer LM (1984) A review of normal tissue hydrogen NMR relaxation times and

relaxation mechanisms from 1-100 MHz: dependence on tissue type, NMR frequency, temperature, species, excision, and age. Med Phys 11:425–448

Butts K, Pauly JM, Gold GE (2005) Reduction of blurring in view angle tilting MRI. Magn Reson Med 53:418–424

Cho ZH, Kim DJ, Kim YK (1988) Total inhomogeneity correction including chemical shifts and susceptibility by view angle tilting. Med Phys 15:7–11

Collins CM, Liu W, Schreiber W, Yang QX, Smith MB (2005) Central brightening due to constructive interference with, without, and despite dielectric resonance. J Magn Reson Imaging 21:192–196

Cruz LC Jr, Sorensen AG (2006) Diffusion tensor magnetic resonance imaging of brain tumors. Magn Reson Imaging Clin N Am 14:183–202

de Bazelaire CM, Duhamel GD, Rofsky NM, Alsop DC (2004) MR imaging relaxation times of abdominal and pelvic tissues measured in vivo at 3.0 T: preliminary results. Radiology 230:652–659

Dietrich O, Reiser MF, Schoenberg SO (2008) Artifacts in 3-T MRI: physical background and reduction strategies. Eur J Radiol 65:29–35

Duewell S, Wolff SD, Wen H, Balaban RS, Jezzard P (1996) MR imaging contrast in human brain tissue: assessment and optimization at 4 T. Radiology 199:780–786

Edelstein WA, Glover GH, Hardy CJ, Redington RW (1986) The intrinsic signal-to-noise ratio in NMR imaging. Magn Reson Med 3:604–618

Foster JR, Hall DA, Summerfield AQ, Palmer AR, Bowtell RW (2000) Sound-level measurements and calculations of safe noise dosage during EPI at 3 T. J Magn Reson Imaging 12:157–163

Franklin KM, Dale BM, Merkle EM (2008) Improvement in B1-inhomogeneity artifacts in the abdomen at 3T MR imaging using a radiofrequency cushion. J Magn Reson Imaging 27:1443–1447

Frayne R, Goodyear BG, Dickhoff P, Lauzon ML, Sevick RJ (2003) Magnetic resonance imaging at 3.0 Tesla: challenges and advantages in clinical neurological imaging. Invest Radiol 38:385–402

Fujii Y, Nakayama N, Nakada T (1998) High-resolution T2-reversed magnetic resonance imaging on a high magnetic field system. Technical note. J Neurosurg 89:492–495

Gabriel C, Gabriel S, Corthout E (1996a) The dielectric properties of biological tissues: I. Literature survey. Phys Med Biol 41:2231–2249

Gabriel S, Lau RW, Gabriel C (1996b) The dielectric properties of biological tissues: III. Parametric models for the dielectric spectrum of tissues. Phys Med Biol 41: 2271–2293

Gabriel S, Lau RW, Gabriel C (1996c) The dielectric properties of biological tissues: II. Measurements in the frequency range 10 Hz to 20 GHz. Phys Med Biol 41:2251–2269

Gold GE, Han E, Stainsby J, Wright G, Brittain J, Beaulieu C (2004) Musculoskeletal MRI at 3.0 T: relaxation times and image contrast. AJR Am J Roentgenol 183:343–351

Gomori JM, Grossman RI, Yu-Ip C, Asakura T (1987) NMR relaxation times of blood: dependence on field strength, oxidation state, and cell integrity. J Comput Assist Tomogr 11: 684–690

Griswold MA, Jakob PM, Heidemann RM, Nittka M, Jellus V, Wang J, Kiefer B, Haase A (2002) Generalized autocalibrating partially parallel acquisitions (GRAPPA). Magn Reson Med 47:1202–1210

Haacke EM, Tkach JA, Parrish TB (1989) Reduction of T2* dephasing in gradient field-echo imaging. Radiology 170: 457–462

Haacke EM, Brown RW, Thompson MR, Venkatesan R (1999) Magnetic resonance imaging - physical principles and sequence design, 1st edn. Wiley, New York

Hand JW, Li Y, Thomas EL, Rutherford MA, Hajnal JV (2006) Prediction of specific absorption rate in mother and fetus associated with MRI examinations during pregnancy. Magn Reson Med 55:883–893

Hennig J, Scheffler K (2001) Hyperechoes. Magn Reson Med 46:6–12

Hennig J, Weigel M, Scheffler K (2003) Multiecho sequences with variable refocusing flip angles: optimization of signal behavior using smooth transitions between pseudo steady states (TRAPS). Magn Reson Med 49:527–535

Hetherington H, Kuzniecky R, Pan J, Mason G, Morawetz R, Harris C, Faught E, Vaughan T, Pohost G (1995) Proton nuclear magnetic resonance spectroscopic imaging of human temporal lobe epilepsy at 4.1 T. Ann Neurol 38:396–404

Hoogenraad FG, Reichenbach JR, Haacke EM, Lai S, Kuppusamy K, Sprenger M (1998) In vivo measurement of changes in venous blood-oxygenation with high resolution functional MRI at 0.95 tesla by measuring changes in susceptibility and velocity. Magn Reson Med 39:97–107

Hoult DI, Phil D (2000) Sensitivity and power deposition in a high-field imaging experiment. J Magn Reson Imaging 12:46–67

Huang H, Zhang J, Wakana S, Zhang W, Ren T, Richards LJ, Yarowsky P, Donohue P, Graham E, van Zijl PC, Mori S (2006) White and gray matter development in human fetal, newborn and pediatric brains. Neuroimage 33:27–38

Hussain SM, Wielopolski PA, Martin DR (2005) Abdominal magnetic resonance imaging at 3.0 T: problem or a promise for the future? Top Magn Reson Imaging 16:325–335

Jesmanowicz A, Bandettini PA, Hyde JS (1998) Single-shot half k-space high-resolution gradient-recalled EPI for fMRI at 3 Tesla. Magn Reson Med 40:754–762

Katscher U, Bornert P, Leussler C, van den Brink JS (2003) Transmit SENSE. Magn Reson Med 49:144–150

Komori T, Narabayashi I, Matsumura K, Matsuki M, Akagi H, Ogura Y, Aga F, Adachi I (2007) 2-[Fluorine-18]-fluoro-2-deoxy-D-glucose positron emission tomography/computed tomography versus whole-body diffusion-weighted MRI for detection of malignant lesions: initial experience. Ann Nucl Med 21:209–215

Kruger G, Kastrup A, Glover GH (2001) Neuroimaging at 1.5 T and 3.0 T: comparison of oxygenation-sensitive magnetic resonance imaging. Magn Reson Med 45:595–604

Kuhl CK, Traber F, Schild HH (2008) Whole-body high-field-strength (3.0-T) MR imaging in clinical practice. Part I. Technical considerations and clinical applications. Radiology 246:675–696

Le Bihan D, Mangin JF, Poupon C, Clark CA, Pappata S, Molko N, Chabriat H (2001) Diffusion tensor imaging: concepts and applications. J Magn Reson Imaging 13:534–546

Le Bihan D, Poupon C, Amadon A, Lethimonnier F (2006) Artifacts and pitfalls in diffusion MRI. J Magn Reson Imaging 24:478–488

Li D, Waight DJ, Wang Y (1998) In vivo correlation between blood T2* and oxygen saturation. J Magn Reson Imaging 8:1236–1239

Menon RS, Ogawa S, Hu X, Strupp JP, Anderson P, Ugurbil K (1995) BOLD based functional MRI at 4 Tesla includes a capillary bed contribution: echo-planar imaging correlates with previous optical imaging using intrinsic signals. Magn Reson Med 33:453–459

Merboldt KD, Finsterbusch J, Frahm J (2000) Reducing inhomogeneity artifacts in functional MRI of human brain activation-thin sections vs gradient compensation. J Magn Reson 145:184–191

Merkle EM, Dale BM (2006) Abdominal MRI at 3.0 T: the basics revisited. AJR Am J Roentgenol 186:1524–1532

Merkle EM, Dale BM, Paulson EK (2006) Abdominal MR imaging at 3T. Magn Reson Imaging Clin N Am 14:17–26

Morakkabati-Spitz N, Schild HH, Kuhl CK, Lutterbey G, von Falkenhausen M, Traber F, Gieseke J (2006) Female pelvis: MR imaging at 3.0 T with sensitivity encoding and flip-angle sweep technique. Radiology 241:538–545

Murtz P, Krautmacher C, Traber F, Gieseke J, Schild HH, Willinek WA (2007) Diffusion-weighted whole-body MR imaging with background body signal suppression: a feasibility study at 3.0 Tesla. Eur Radiol 17:3031–3037

Narayana PA, Brey WW, Kulkarni MV, Sievenpiper CL (1988) Compensation for surface coil sensitivity variation in magnetic resonance imaging. Magn Reson Imaging 6:271–274

Ogawa S, Lee TM (1990) Magnetic resonance imaging of blood vessels at high fields: in vivo and in vitro measurements and image simulation. Magn Reson Med 16:9–18

Ojemann JG, Akbudak E, Snyder AZ, McKinstry RC, Raichle ME, Conturo TE (1997) Anatomic localization and quantitative analysis of gradient refocused echo-planar fMRI susceptibility artifacts. Neuroimage 6:156–167

Pruessmann KP, Weiger M, Scheidegger MB, Boesiger P (1999) SENSE: sensitivity encoding for fast MRI. Magn Reson Med 42:952–962

Reichenbach JR, Venkatesan R, Schillinger DJ, Kido DK, Haacke EM (1997) Small vessels in the human brain: MR venography with deoxyhemoglobin as an intrinsic contrast agent. Radiology 204:272–277

Reichenbach JR, Essig M, Haacke EM, Lee BC, Przetak C, Kaiser WA, Schad LR (1998) High-resolution venography of the brain using magnetic resonance imaging. MAGMA 6:62–69

Ren T, Anderson A, Shen WB, Huang H, Plachez C, Zhang J, Mori S, Kinsman SL, Richards LJ (2006) Imaging, anatomical, and molecular analysis of callosal formation in the developing human fetal brain. Anat Rec A Discov Mol Cell Evol Biol 288:191–204

Sbarbati A, Pizzini F, Fabene PF, Nicolato E, Marzola P, Calderan L, Simonati A, Longo L, Osculati A, Beltramello A (2004) Cerebral cortex three-dimensional profiling in human fetuses by magnetic resonance imaging. J Anat 204:465–474

Soher BJ, Dale BM, Merkle EM (2007) A review of MR physics: 3T versus 1.5T. Magn Reson Imaging Clin N Am 15:277–290, v

Stadlbauer A, Bernt R, Gruber S, Bogner W, Pinker K, van der Riet W, Haller J, Salomonowitz E (2009) Diffusion-weighted MR imaging with background body signal suppression (DWIBS) for the diagnosis of malignant and benign breast lesions. Eur Radiol 19:2349–2356

Stanisz GJ, Odrobina EE, Pun J, Escaravage M, Graham SJ, Bronskill MJ, Henkelman RM (2005) T1, T2 relaxation and magnetization transfer in tissue at 3T. Magn Reson Med 54:507–512

Takahara T, Imai Y, Yamashita T, Yasuda S, Nasu S, Van Cauteren M (2004) Diffusion weighted whole body imaging with background body signal suppression (DWIBS): technical improvement using free breathing, STIR and high resolution 3D display. Radiat Med 22:275–282

Takahara T, Hendrikse J, Yamashita T, Mali WP, Kwee TC, Imai Y, Luijten PR (2008) Diffusion-weighted MR neurography of the brachial plexus: feasibility study. Radiology 249:653–660

Tanenbaum LN (2006) Clinical 3T MR imaging: mastering the challenges. Magn Reson Imaging Clin N Am 14:1–15

Thulborn KR (1999) Clinical rationale for very-high-field (3.0 Tesla) functional magnetic resonance imaging. Top Magn Reson Imaging 10:37–50

Thulborn KR, Waterton JC, Matthews PM, Radda GK (1982) Oxygenation dependence of the transverse relaxation time of water protons in whole blood at high field. Biochim Biophys Acta 714:265–270

Turner R, Jezzard P, Wen H, Kwong KK, Le Bihan D, Zeffiro T, Balaban RS (1993) Functional mapping of the human visual cortex at 4 and 1.5 tesla using deoxygenation contrast EPI. Magn Reson Med 29:277–279

Ugurbil K, Garwood M, Ellermann J, Hendrich K, Hinke R, Hu X, Kim SG, Menon R, Merkle H, Ogawa S et al (1993) Imaging at high magnetic fields: initial experiences at 4 T. Magn Reson Q 9:259–277

Ullmann P, Junge S, Wick M, Seifert F, Ruhm W, Hennig J (2005) Experimental analysis of parallel excitation using dedicated coil setups and simultaneous RF transmission on multiple channels. Magn Reson Med 54:994–1001

Vernickel P, Roschmann P, Findeklee C, Ludeke KM, Leussler C, Overweg J, Katscher U, Grasslin I, Schunemann K (2007) Eight-channel transmit/receive body MRI coil at 3T. Magn Reson Med 58:381–389

Vinitski S, Griffey RH (1991) MR image contrast at high field strength. J Magn Reson Imaging 1:451–456

Weigel M, Hennig J (2006) Contrast behavior and relaxation effects of conventional and hyperecho-turbo spin echo sequences at 1.5 and 3 T. Magn Reson Med 55:826–835

Wen H, Denison TJ, Singerman RW, Balaban RS (1997) The intrinsic signal-to-noise ratio in human cardiac imaging at 1.5, 3, and 4 T. J Magn Reson 125:65–71

Wieben O, Francois C, Reeder SB (2008) Cardiac MRI of ischemic heart disease at 3 T: potential and challenges. Eur J Radiol 65:15–28

Yablonskiy DA, Haacke EM (1994) Theory of NMR signal behavior in magnetically inhomogeneous tissues: the static dephasing regime. Magn Reson Med 32:749–763

Zhu Y (2004) Parallel excitation with an array of transmit coils. Magn Reson Med 51:775–784